

Structure of Al(111)-(2×2)-Rb

D. L. Adams, M. M. Nielsen, and J. Burchardt

Institute of Physics and Astronomy, Aarhus University, DK-8000 Aarhus C, Denmark

J. N. Andersen

Department of Synchrotron Radiation Research, Institute of Physics, Lund University, S-223 62 Lund, Sweden

(Received 11 June 1999)

The atomic geometry of the Al(111)-(2×2)-Rb phase formed by adsorption of one-quarter monolayer Rb on Al(111) at 100 K has been determined by analysis of low-energy electron diffraction measurements. The adsorbed Rb atoms are found to occupy on-top sites on a rumpled first layer of Al atoms, as in the corresponding $(\sqrt{3}\times\sqrt{3})R30^\circ$ phases formed by adsorption of one-third monolayer K, Rb, and Cs on Al(111) at low temperature. However, the adsorbed Rb atoms in the (2×2) phase have anomalously large thermal vibrations. [S0163-1829(99)04939-5]

I. INTRODUCTION

The discovery of the reconstructive adsorption of Al(111) by adsorption of Na, as reported¹ in a surface extended x-ray absorption (SEXAFS) study in 1991, stimulated a renewed interest in the adsorption of alkali metals on Al surfaces. Subsequent studies^{2,3} have revealed an unexpected richness of structural phenomena for these electronically simple systems. Thus it has been found that adsorption of alkali metals on Al surfaces at room temperature leads in general to a reconstruction of the substrate, with formation of substitutional, binary surface alloys. Studies of the coadsorption of alkali metals have further revealed the occurrence of ternary surface alloys. Adsorption of alkali metals at low temperature leads in general to the formation of chemisorbed structures, although for several systems strong perturbations of the substrate atom positions occur, such that these systems can perhaps be regarded as weak reconstructions. Finally, order-order and, in some cases, order-preserving, irreversible phase transformations have been found between chemisorbed and reconstructed structures.

Most of the work carried out to date has been on the Al(111) surface where structure determinations have been reported^{1,3,4} for most of the 15 known well-ordered adsorbed phases, although substitutional adsorption of Li and Na has also been found recently⁵⁻⁷ on Al(100) and Al(110). In the present paper, we report on the structure of the (2×2)-Rb phase formed by adsorption of one-quarter monolayer Rb on Al(111) at 100 K. It will be shown that the structure of this phase is similar to the structures of the corresponding Al(111)- $(\sqrt{3}\times\sqrt{3})R30^\circ$ -K, Rb, and Cs phases⁸⁻¹¹ formed by adsorption of one-third monolayer K, Rb, and Cs at 100 K, but that the vibrational amplitudes of the adsorbed Rb atoms in the (2×2) phase are anomalously large. In the present paper only isotropic vibrations have been considered. In a forthcoming article, Moritz and Landskron¹² report a more detailed analysis of the vibrations, which indicates the occurrence of a large anisotropy.

II. EXPERIMENTAL

The measurements were carried out in a Vacuum Generators mu-metal ultrahigh vacuum chamber with base pressure

of 3×10^{-11} torr. Low-energy electron diffraction (LEED) intensity measurements were carried out using an Omicron reverse-view LEED optics and a video-LEED system described previously.^{13,14} Rb was deposited onto the crystal by evaporation from a (SAES) Getters source.¹⁵ The deposition was carried out in a few minutes and the residual-gas pressure during evaporation was typically 2×10^{-10} torr. Sharp (2×2) LEED patterns with good contrast were obtained after deposition of 1/4 monolayer at 100 K. Optimum development of the (2×2) structure was achieved by incremental deposition of Rb until a maximum was reached in the ratio of integrated intensity in fractional-order and integral-order diffracted beams. Auger electron spectroscopy measurements taken after deposition and after completion of a set of LEED measurements indicated that surface contamination (almost entirely C) was less than 0.03 monolayer.

Intensity-energy spectra were measured for the (2×2) structure at 100 K at normal incidence in the energy range 40–400 eV with a step size of 1 eV. Intensity-energy spectra were measured for a total of 14 symmetry-inequivalent beams (5 integral-order beams and 9 fractional-order beams). The measured intensities were corrected for the background intensity, the variation of the incident beam current with energy, the variation of the spot intensity with position on the fluorescent screen of the LEED optics, and the spatial response of the video camera.¹⁴ The intensities of all beams are on the same, accurately defined, although arbitrary, intensity scale.

III. LEED CALCULATIONS

LEED intensities were calculated using the dynamical theory of LEED, with computer programs¹⁶ derived originally from the layer-doubling and combined-space programs of Pendry¹⁷ and of Van Hove and Tong.¹⁸ Scattering phase shifts for Al and Rb were calculated from the muffin-tin band-structure potentials of Moruzzi *et al.*¹⁹ Atomic scattering matrices were renormalized for the effects of thermal vibrations using isotropic, root-mean-square (rms) vibrational amplitudes u_{Rb} for the adsorbed Rb atoms, and u_{Al_1} , u_{Al_2} , and $u_{Al_{bulk}}$ for Al atoms in the first, second, and bulk

layers, respectively, as described in the Appendix. In most of the calculations, up to 196 partial waves (14 phase shifts, $l_{\max}=13$) and 283 plane waves (reduced by symmetry to 56 symmetry-adapted plane waves) were used in the L -space and k -space treatments, respectively, of multiple scattering within and between layers parallel to the surface. The complex electron self energy $\Sigma = V_0 + iV_{im}$ was taken to be independent of energy. The surface potential barrier was taken to be a refracting but nonreflecting step of height V_0 , positioned at a distance equal to one-half the bulk interlayer spacing above the first layer of atoms.

As described in the next section, anomalously large vibrational amplitudes were found for the adsorbed Rb atoms. It was found that the use of standard algorithms^{17,18} gave rise to serious errors in the diffracted intensities for vibrational amplitudes greater than ~ 0.3 Å. This necessitated modifications to the algorithm for the calculation of the Bessel functions that are required in the calculation of the temperature-dependent atomic t matrices, as described in the Appendix.

In the final stage of the structural refinement, the convergence of the intensity calculations was checked with respect to the number of phase shifts for both Al and Rb. Whereas the intensities were found to be converged to better than 2% using 14 phase shifts for Al, more phase shifts were required to obtain the same level of convergence for Rb. Thus, the final refinement was carried out using 21 phase shifts for Rb. The resulting changes in the optimum values of the structural and nonstructural variables were, however, within the estimated uncertainties.

IV. SURFACE STRUCTURE DETERMINATION

The analysis of the present LEED measurements for the (2×2)-Rb phase was started after the structure determinations⁸⁻¹⁰ for the low-temperature Al(111)-($\sqrt{3}\times\sqrt{3}$)R30°- K and Rb phases had been carried out. It was natural to expect that the adsorbed alkalis in the (2×2) phases would occupy the same on-top sites found for the ($\sqrt{3}\times\sqrt{3}$)R30° phases, although there had been suggestions based on total-energy calculations²⁰ that the adsorbed alkalis might occupy fcc sites at low coverage. However, our first attempts at analysis of the (2×2) phase in terms of occupation of on-top sites were unsuccessful, so a detailed investigation of other structural models was carried out, including alkali atoms adsorbed in threefold hollow fcc and hcp sites, and sixfold substitutional sites, compatible with the symmetry of the measured LEED intensities. A common feature of these early trials was the observation that for several structural models a reasonable level of agreement could be obtained between experimental and calculated spectra for the integral-order beams, whereas poor or no correspondence was found for the fractional-order beams. The early calculations were carried out using values for u_{Rb} in the range 0.2-0.3 Å, as found previously for the Al(111)-($\sqrt{3}\times\sqrt{3}$)R30°- K and Rb on-top structures.⁸⁻¹⁰ Attempts to increase the range over which u_{Rb} was varied led to discontinuities in plots of the R factor for the disagreement between theory and experiment, defined below, versus u_{Rb} , which were finally traced to serious errors in the calculations of diffracted intensities for values of vibrational amplitudes greater than ~ 0.3 Å. After solution of this problem, as discussed in the

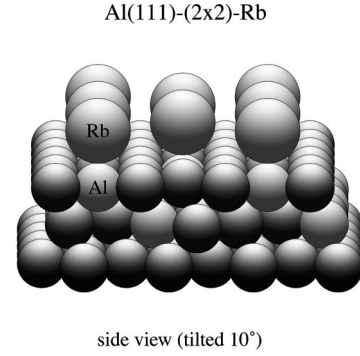


FIG. 1. Hard-sphere model of the geometry of the Al(111)-(2×2)-Rb structure. Side view, shown as a central projection on the ($\bar{1}\bar{1}2$) plane tilted by 10° with respect to the plane of the paper.

Appendix, satisfactory agreement between experimental and calculated intensities was obtained for models involving Rb adsorbed in on-top sites with large thermal vibrations.

A full optimization of the fit between experimental intensities and intensities calculated for Rb adsorbed in the on-top site was then carried out using a semi-automatic implementation of an iterative procedure described previously,^{4,16} in which the disagreement between experimental and calculated intensities, as measured by an R factor, is minimized as a function of one variable at a time. The R factor is a normalized χ^2 function defined^{4,14,21} as:

$$R = \sum_{hk,i} \left(\frac{I_{hk,i}^{ex} - c I_{hk,i}^{cal}}{\sigma_{hk}} \right)^2 \bigg/ \sum_{hk,i} \left(\frac{I_{hk,i}^{ex}}{\sigma_{hk}} \right)^2, \quad (1)$$

where c is a *global* scaling constant between the experimental $I_{hk}^{ex}(E)$ and calculated intensities $I_{hk}^{cal}(E)$, and σ_{hk} is the root-mean-square experimental uncertainty of the beam hk , obtained⁴ via comparison of measurements for (nominally) symmetry-equivalent beams. The scaling constant c is determined by the requirement that $\partial R / \partial c = 0$ as

$$c = \sum_{hk,i} \left(\frac{I_{hk,i}^{ex} I_{hk,i}^{cal}}{\sigma_{hk}^2} \right) \bigg/ \sum_{hk,i} \left(\frac{I_{hk,i}^{cal}}{\sigma_{hk}} \right)^2. \quad (2)$$

Substitution for c in Eq. (1) leads to

$$R = 1 - \left[\sum_{hk,i} \left(\frac{I_{hk,i}^{ex} I_{hk,i}^{cal}}{\sigma_{hk}} \right) \right]^2 \bigg/ \sum_{hk,i} \left(\frac{I_{hk,i}^{ex}}{\sigma_{hk}} \right)^2 \sum_{hk,i} \left(\frac{I_{hk,i}^{cal}}{\sigma_{hk}} \right)^2, \quad (3)$$

from which it follows that R is bounded by 0 and 1.

A hard-sphere model of the resulting structure of the Al(111)-(2×2)-Rb phase is shown in Fig. 1, and the detailed results of the refinement are listed in Table I. It can be seen from the table and from the model, that the first Al layer is rumpled. Al atoms directly beneath adsorbed Rb atoms are displaced vertically towards the bulk by Δr_1 with respect to the remaining Al atoms of the layer. In the final stage of the analysis the possibility of relaxations of the atomic positions in the second Al layer was also investigated. As can be seen from the table, it was found that Al atoms closest to the rotational axis through the adsorbed alkali atoms were found to be displaced radially by Δa_2 away from the axis in the plane parallel to the surface, whereas the remaining atoms in

TABLE I. Best-fit parameter values for Rb adsorbed in the on-top site in the Al(111)-(2×2)-Rb structures. The interlayer spacings are denoted d_j and the vibrational amplitudes are denoted u_j . $d_{alkali-Al_1}$ is the vertical spacing from the alkali layer to the midpoint of the first, rumpled Al layer. $d_{Al_1-Al_2}$ is the vertical spacing from the midpoint of the first, rumpled Al layer to the midpoint of the second, rumpled Al layer. Δr_1 is the vertical spacing between the two subplanes in the first rumpled layer. Δr_2 is the vertical spacing between the two subplanes in the second rumpled layer, and Δa_2 is the lateral displacements of atoms in the lower subplane of the second rumpled layer (see text). Where appropriate, the corresponding values (Ref. 21) for the clean Al(111) surface are also listed for comparison.

Parameter	(1×1)	(2×2)-Rb
$d_{alkali-Al_1}$		$3.21 \pm 0.26 \text{ \AA}$
Δr_{Al_1}		$0.22 \pm 0.03 \text{ \AA}$
$d_{Al_1-Al_2}$	$2.36 \pm 0.01 \text{ \AA}$	$2.30 \pm 0.02 \text{ \AA}$
Δr_{Al_2}		$0.04 \pm 0.02 \text{ \AA}$
Δa_{Al_2}		$0.03 \pm 0.04 \text{ \AA}$
$d_{Al_2-Al_3}$	$2.33 \pm 0.01 \text{ \AA}$	$2.33 \pm 0.03 \text{ \AA}$
$d_{Al_3-Al_4}$	$2.32 \pm 0.01 \text{ \AA}$	$2.33 \pm 0.03 \text{ \AA}$
u_{alkali}		$1.11 \pm 0.15 \text{ \AA}$
u_{Al_1}	$0.13 \pm 0.02 \text{ \AA}$	$0.18 \pm 0.02 \text{ \AA}$
u_{Al_2}	$0.08 \pm 0.01 \text{ \AA}$	$0.11 \pm 0.02 \text{ \AA}$
$u_{Al_{bulk}}$	$0.08 \pm 0.01 \text{ \AA}$	$0.11 \pm 0.01 \text{ \AA}$
V_{im}	$4.0 \pm 0.4 \text{ eV}$	$3.6 \pm 0.8 \text{ eV}$
R	0.009	0.051

the second layer were found to be displaced vertically by Δr_2 towards the surface. We emphasize, however, that the uncertainties for these displacements are of the order of the displacements themselves.

Perhaps the most surprising aspect of the analysis is the observation of very large vibrational amplitudes for the adsorbed alkalis, although we note that quite large amplitudes have also been reported²² recently for alkalis adsorbed on Ag(111). It can also be noted that the enhanced vibrational amplitudes of Al atoms in the first layer of the clean Al(111) substrate persist after adsorption of Rb. Similar observations were made previously⁸⁻¹⁰ for the corresponding ($\sqrt{3} \times \sqrt{3}$)R30°-K, and Rb structures.

Plots of experimental intensity spectra and spectra calculated for the optimum parameter values given in Table I are shown in Fig. 2. The very good agreement between experiment and theory for the integral-order beams is close to the level of the reproducibility of the measurements, as determined by comparisons of intensity spectra for (nominally) symmetry-equivalent beams. A reasonably good level of agreement is obtained for the fractional-order beams, except for the (0, $\bar{1}/2$) beam, where significant differences can be seen between the experimental and theoretical line-shapes. We note that the plots have been constructed using a single, beam-independent, scaling factor between experiment and calculations. Thus the agreement between experiment and theory also includes agreement between the relative intensities of the different beams. As can be seen from the scale factors in Fig. 2, the maximum intensities of the different beams span ranges of about 26.

V. SUMMARY AND CONCLUSIONS

In summary, the present paper has shown that the Al(111)-(2×2)-Rb phase formed by adsorption of 1/4 monolayer of Rb on Al(111) at low temperature consists of Rb atoms adsorbed in on-top sites on a rumpled Al layer, in which Al atoms directly beneath the adsorbed alkali atoms are displaced by 0.22 Å towards the bulk with respect to the remaining Al atoms in the first layer. The inward displacements of Al atoms in the first layer of the substrate give rise to small lateral and vertical displacements of Al atoms in the second layer. The corresponding hard-sphere radii of the Rb atoms are 1.89 Å, as compared to the bulk (bcc) metallic radius²³ of 2.47 Å. The vibrational amplitudes of adsorbed Rb atoms of 1.13 Å are extremely large. As described in a forthcoming article by Moritz and Landskron,¹² a more detailed analysis, in which the restriction of isotropic vibrations is relaxed, indicates that the vibrations are largely parallel to the surface.

ACKNOWLEDGMENTS

The authors would like to thank Wolfgang Moritz for useful discussions. Support of this work by the Danish Natural Science Research Council is gratefully acknowledged.

APPENDIX

As noted in Sec. III, serious errors were found in the calculation of LEED intensities for vibrational amplitudes of the adsorbed alkali atoms greater than $\sim 0.3 \text{ \AA}$. These errors were traced to errors in the calculation of the spherical Bessel functions used in the calculation of the temperature-dependent atomic t matrices. Much of the core computer code used in our calculations, including the calculation of the temperature-dependent atomic t matrices, stems from the pioneering work of Pendry,¹⁷ as extended by Van Hove and Tong.¹⁸ Since this is also true to our knowledge for the code used by other workers in the field, we believe that it is appropriate to describe a simple solution to this problem.

The temperature-dependent atomic t matrices t_l are given in terms of the corresponding matrices for zero temperature t_l^0 by rewriting Eq. (6.65) in Ref. 17 as

$$t_l = \exp(z) \sum_L^{2l_{\max}+1} \sum_{l'}^{l_{\max}} \{i^l j_L(iz) [4\pi(2L+1)(2l'+1) \times (2l+1)^{-1}]^{1/2} B^{l'}(L0, l0)\} t_{l'}^0, \quad (\text{A1})$$

where j_L is a spherical Bessel function, with argument $z = -(1/3)u^2 k^2$. The isotropic, rms vibrational amplitude of the atom in question is u , that is, if \mathbf{u} is the displacement of an atom from its node at a given instant, then its time-average value is given by $u^2 = u_1^2 + u_2^2 + u_3^2$ ($= 3u_1^2$, for isotropic vibrations) where $u_{1,2,3}$ are the time-average values of the projection of \mathbf{u} on three orthogonal axes.²⁴ (We note that the mean-square vibrational amplitude u^2 can be related to a Debye temperature²⁴ θ_D via $u^2 = 9\hbar^2 T / M k_B \theta_D^2 [(\theta_D/4T) + \varphi(\theta_D/T)]$, where the function $\varphi(\theta_D/T)$ is defined in Ref. 24. However, the vibrational amplitudes u rather than the Debye temperatures θ_D are the direct input to our calculations, and are optimized in the structural refinement.)] The

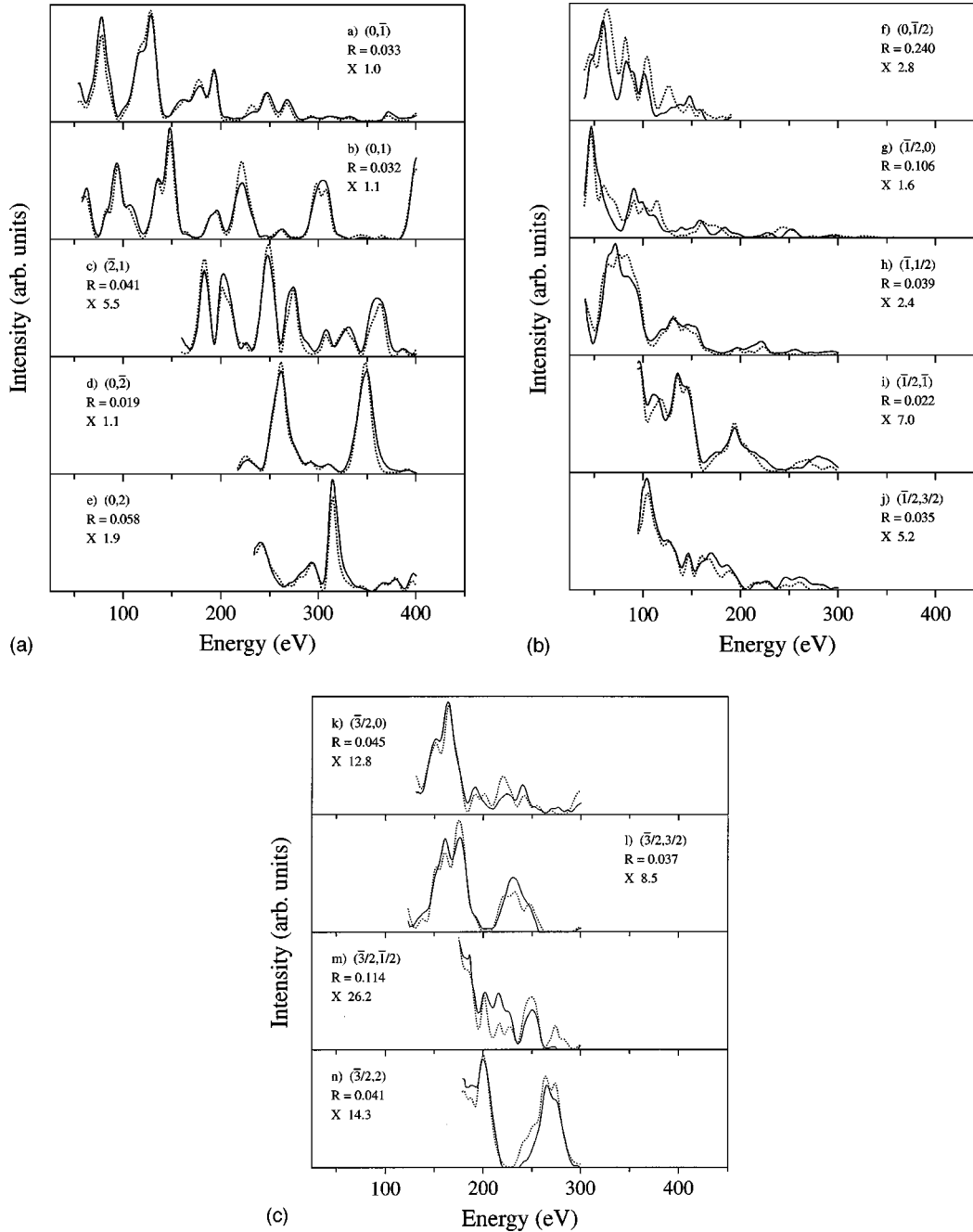


FIG. 2. Comparison of experimental (solid lines) and calculated (dotted lines) intensity-energy spectra for Al(111)-(2×2)-Rb for 5 integral-order beams, (a)–(e), and 9 fractional order beams, (f)–(n). The beam hk indices, R factors, and scale factors are shown in each panel. Multiplication of the intensities in each panel by the scale factors shown would bring the intensities on to the same accurately known, although arbitrary, intensity scale. The calculated spectra were obtained using the best-fit parameter values given in Table I.

real part of the electron wave vector in the solid is $k^2 = E$ for electron energy E . The maximum number of phase shifts used in the calculations is $l_{\max} + 1$. The $B^{l'}(L0, l0)$ are Clebsch-Gordon coefficients defined by Eq. (4.40) in Ref. 17. The zero-temperature atomic t-matrix t_l^0 in Eq. (A1) is given in terms of the scattering phase-shifts δ_l^0 by $t_l^0 = [\exp(2i\delta_l^0) - 1]/2$. We note that Pendry's original code used Eq. (A1) to calculate temperature-dependent phase-shifts δ_l defined by: $t_l = [\exp(2i\delta_l) - 1]/2$ for later use in calculating t_l . The intermediate calculation of temperature-dependent phase-shifts is still performed in more recent programs,¹⁸

even when the δ_l are not saved for use in subsequent program runs. This requires a complex logarithm in calculating the δ_l from the t_l followed by a complex exponential in calculating the t_l from the δ_l . This redundancy is not present in our programs, which calculate the t_l directly from Eq. (A1).

Calculation of the spherical Bessel function j_l in Eq. (A1) can be carried out by the upward recursion

$$j_{l+1} = (2l+1)(iz)^{-1}j_l - j_{l-1} \quad (\text{A2})$$

from the starting values:

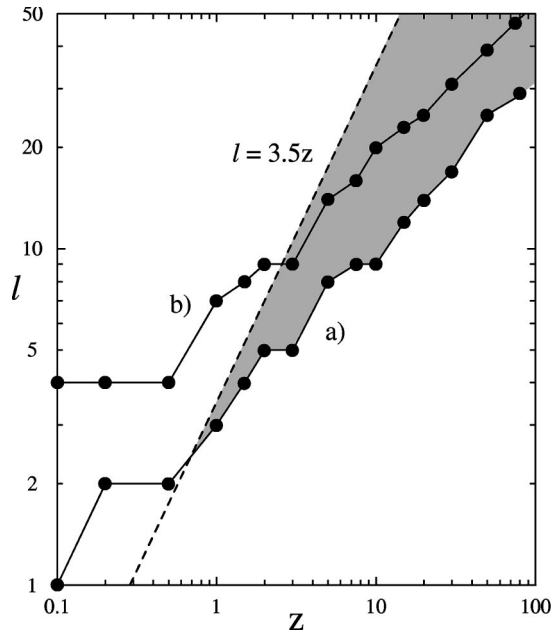


FIG. 3. Plot of the maximum value of l , for which the calculation of the spherical Bessel functions $j_l(iz)$ is accurate to 0.1%, versus z . (a) single-precision calculations. (b) double-precision calculations. The shaded triangular region in the figure is the region for which Pendry's algorithm still uses the upward recursion, but where the recursion fails (see text).

$$j_0 = (iz)^{-1} \sin(iz); \quad j_1 = (iz)^{-2} \sin(iz) - (iz)^{-1} \cos(iz). \quad (\text{A3})$$

However, as noted by Pendry (Ref. 17, p. 271), the upward recursion for $j_l(iz)$ is unstable at small z . Thus, in Pendry's algorithm, as also used by Van Hove and Tong,¹⁸ $j_l(iz)$ is calculated by upward recursion for $l \leq l_{cut}$ and by using the first three terms of a series expansion [Eq. (10.1.2) in Ref. 25] for $l > l_{cut}$, where $l_{cut} = 3.5z$.

Pendry's algorithm for calculation of $j_l(iz)$ gives accurate results for $z \leq 1.5$, corresponding to "normal" vibrational amplitudes and energies ($z = 1.5$ corresponds to $u = 0.20 \text{ \AA}$ at $E = 410 \text{ eV}$). However, as shown in Fig. 3, the algorithm fails for larger z , if the calculations are carried out in single precision, where the condition $l_{cut} = 3.5z$ is not sufficiently strict. In Fig. 3, the maximum value of l for which the upward recursion is accurate to better than 0.1% is plotted against z , for both single-precision and double-precision cal-

culations. We emphasize that although the 0.1% measure of accuracy is arbitrary, the error increases catastrophically for values of l greater than those plotted for given z . The condition $l_{cut} = 3.5z$ is shown as a dotted line on the figure. The shaded triangular region in the figure is the region for which Pendry's algorithm still uses the upward recursion, but where the recursion fails. As can be seen from the figure, the region of failure is reduced, but not eliminated by carrying out the calculations in double precision. The results shown in the figure could in principle be used to define an appropriate relation between l_{cut} and z . It turns out, however, that reducing l_{cut} leads to inaccuracies in calculating $j_l(iz)$ for $l > l_{cut}$ if only the first three terms of the series expansion are used.

The solution to the difficulties noted above is to carry out a simple downward recursion for all values of l and z , using a procedure attributed to J. C. P. Miller (Section 10.5 in Ref. 25). The recursion is started by defining $j_l = 0$ and $j_{l-1} = 1$ for a value of l larger than the maximum value required. In our implementation we take this starting value to be simply twice the maximum required value of l , and carry out a downward recursion leading to j_1 . The values obtained in the downward recursion are then renormalized by the ratio of the value of j_1 from the recursion to the value obtained from Eq. (A3). For convenience we calculate $i^l j_l(iz) = (-1)^l I_l(z)$, where $I_l(z)$ is a modified spherical Bessel function, since $I_l(z)$ is real for real z . $I_l(z)$ for $l=0,1$ is given by

$$I_0 = (z)^{-1} \sinh(z); \quad I_1 = -(z)^{-2} \sinh(z) + (z)^{-1} \cosh(z) \quad (\text{A4})$$

and the recursion relation is

$$I_{l+1} = I_{l-1} - (2l+1)(z)^{-1} I_l. \quad (\text{A5})$$

The algorithm is implemented in double precision to avoid overflow in the calculation of $I_l(z)$ at large (negative) values of z , and yields values in agreement with those given in Table 10.10 in Ref. 25 for values of l and z up to 100, to the 10 significant figures given in the table. Finally, we note that the summation of Eq. (A1) is also carried out in double precision to avoid underflow in the calculation of $\exp(z)$ at large z . Fortran subroutines BESITR and TMATK, which implement, respectively, the downward recursion calculation of the Bessel functions, and the temperature-dependent atomic t matrices, are available on request from the first author.

¹A. Schmalz, S. Aminpirooz, L. Becker, J. Haase, J. Neuegebauer, M. Scheffler, D. R. Batchelor, D. L. Adams, and E. Bøgh, Phys. Rev. Lett. **67**, 2163 (1991).

²J. N. Andersen, Surf. Rev. Lett. **2**, 345 (1995), and references therein.

³D. L. Adams, Appl. Phys. **62**, 123 (1996), and references therein.

⁴M. M. Nielsen, S. V. Christensen, and D. L. Adams, Phys. Rev. B **54**, 17 902 (1996).

⁵W. Berndt, D. Weick, C. Stampfl, A. M. Bradshaw, and M. Scheffler, Surf. Sci. **330**, 182 (1995).

⁶J. H. Petersen, A. Mikkelsen, M. M. Nielsen, and D. L. Adams,

Phys. Rev. B **60**, 5963 (1999).

⁷A. Mikkelsen, J. Jiruse, S. V. Hoffmann, J. Petersen, and D. L. Adams (unpublished).

⁸C. Stampfl, M. Scheffler, H. Over, J. Burchhardt, M. M. Nielsen, D. L. Adams, and W. Moritz, Phys. Rev. Lett. **69**, 1532 (1992).

⁹C. Stampfl, M. Scheffler, H. Over, J. Burchhardt, M. M. Nielsen, D. L. Adams, and W. Moritz, Phys. Rev. B **49**, 4959 (1992).

¹⁰M. M. Nielsen, J. Burchhardt, D. L. Adams, E. Lundgren, and J. N. Andersen, Phys. Rev. Lett. **72**, 3370 (1994).

¹¹M. M. Nielsen, J. Burchhardt, D. L. Adams, and J. N. Andersen, Phys. Rev. B **58**, 12 655 (1998).

- ¹²W. Moritz and J. Landskron (unpublished).
- ¹³D. L. Adams, S. P. Andersen, and J. Burchhardt, in *The Structure of Surfaces III*, edited by S. Y. Tong, M. A. V. Hove, X. Xide, and K. Takayanagi (Springer, Berlin, 1991), p. 156.
- ¹⁴M. M. Nielsen, J. Burchhardt, and D. L. Adams, *Phys. Rev. B* **50**, 7851 (1994).
- ¹⁵SAES Getters, Milan, Italy.
- ¹⁶D. L. Adams, V. Jensen, X. F. Sun, and J. H. Vollesen, *Phys. Rev. B* **38**, 7913 (1988).
- ¹⁷J. B. Pendry, *Low Energy Electron Diffraction* (Academic Press, London, 1974).
- ¹⁸M. A. V. Hove and S. Y. Tong, *Surface Crystallography by LEED* (Springer-Verlag, Berlin, 1979).
- ¹⁹V. L. Moruzzi, J. F. Janak, and A. R. Williams, *Calculated Electronic Properties of Metals* (Pergamon, New York, 1978).
- ²⁰J. Neugebauer and M. Scheffler, *Phys. Rev. Lett.* **71**, 577 (1992).
- ²¹J. Burchhardt, M. M. Nielsen, D. L. Adams, E. Lundgren, and J. N. Andersen, *Phys. Rev. B* **50**, 4718 (1994).
- ²²G. S. Leatherman, R. D. Diehl, P. Kaukasoina, and M. Lindroos, *Phys. Rev. B* **53**, 10 254 (1996).
- ²³A. Taylor and B. J. Kagle, *Crystallographic Data on Metal and Alloy Structures* (Dover, New York, 1963).
- ²⁴A. Guinier, *X-Ray Diffraction* (Freeman, San Francisco, 1963).
- ²⁵*Handbook of Mathematical Functions*, edited by M. Abramowitz and I. A. Stegun (Dover, New York, 1970), p. 452.